Atmos. Meas. Tech. Discuss., https://doi.org/10.5194/amt-2018-435
Manuscript under review for journal Atmos. Meas. Tech.
Discussion started: 7 January 2019

Atmospheric Measurement Techniques
Open Access
Discussions

Revisiting particle sizing using grayscale optical array probes: evaluation using laboratory experiments and synthetic data

Sebastian J. O'Shea[1], Jonathan Crosier[1,2], James Dorsey[1,2], Waldemar Schledewitz[1], Ian Crawford[1], Stephan Borrmann[3,4] Richard Cotton[5] and Aaron Bansemer[6]

[1]{School of Earth and Environmental Sciences, University of Manchester, Manchester, UK}

[2]{National Centre for Atmospheric Science, University of Manchester, Manchester, UK}

[3]{Particle Chemistry Department, Max Planck Institute for Chemistry, Mainz, Germany}

[4]{Institute for Atmospheric Physics, Johannes Gutenberg University, Mainz, Germany}

[5]{Met Office, Exeter, UK}

[6]{National Center for Atmospheric Research, Boulder CO, USA}

Correspondence to: S. J. O'Shea (sebastian.oshea@manchester.ac.uk)

Abstract

In-situ observations from research aircraft and instrumented ground sites are important contributions to developing our collective understanding of clouds, and are used to inform and validate numerical weather and climate models. Unfortunately, biases in these datasets may be present, which can limit their value. In this paper, we discuss artefacts which may bias data from a widely used family of instrumentation in the field of cloud physics, Optical Array Probes (OAPs). Using laboratory and synthetic datasets, we demonstrate how greyscale analysis can be used to filter data, constraining the sample volume of the OAP, and improving data quality particularly at small sizes where OAP data are considered unreliable. We apply the new methodology to ambient data from two contrasting case studies: one warm cloud and one cirrus cloud. In both cases the new methodology reduces the concentration of small particles (< 60 µm) by approximately an order of magnitude. This significantly improves agreement with a Mie scattering spectrometer for the liquid case and with a holographic imaging probe for the

Atmos. Meas. Tech. Discuss., https://doi.org/10.5194/amt-2018-435
Manuscript under review for journal Atmos. Meas. Tech.
Discussion started: 7 January 2019

cirrus case. Based on these results, we make specific recommendations to instrument manufacturers, instrument operators, and data processors about the optimal use of greyscale OAP's. We also raise the issue of bias in OAP's which have no greyscale capability.

1 Introduction

Optical array probes (OAPs) are widely used to provide in situ measurements of cloud particle size, habit and concentration (Wendisch and Brenguier, 2013). These measurements provide insights into key cloud microphysical processes such as ice nucleation, particle growth and precipitation (Field, 1999; Lawson et al., 2015). In situ measurements are an important means to validate remote sensing instrumentation, which are routinely used to initialise operational weather forecast models (Fox et al., 2018; Mace & Benson, 2017).

OAPs consist of a laser illuminating a linear array of photo-diodes. A particle crossing the laser beam is detected if the laser intensity at any of the elements of the array drops below a threshold value. A shadow image is constructed by appending consecutive slices from the detectors as the particle moves perpendicular to the laser beam.

Monoscale OAPs use a 50% decrease in signal intensity as their threshold for detection (Lawson et al., 2006), resulting in 1-bit binary images with pixels either in an active state, or an inactive state. Greyscale OAPs are also available, which detect particles at multiple intensity thresholds, resulting in 2-bit images with pixels having three different active states, and one in-active state. For example, a greyscale probe could be configured to record images with pixels off (inactive), or triggered at shadow intensity levels of 25%, 50% and 75%. We use the abbreviations A_{25-50}, A_{50-75} and A_{75-100} for the number of pixels associated with a decrease in detector signal of 25 – 50%, 50 – 75% and 75 – 100%, respectively. Similarly we use the abbreviations D_{25}, D_{50}, and D_{75} for the diameter of images with decreases in detector signal greater than 25, 50 and 75%, respectively. Korolev et al. (1991) describes a hybrid mono-grey system for the closely related 1-D type of probe; this used a similar array as an OAP to size particles using a 50% shadow intensity, but also had on-board signal processing to provide additional filtering and the requirement for at least 1 pixel in any measured image to have a shadow intensity >67%. This resulted in the reduction of artefacts due to poorly imaged particles near the edges of the depth of field.

Atmos. Meas. Tech. Discuss., https://doi.org/10.5194/amt-2018-435
Manuscript under review for journal Atmos. Meas. Tech.
Discussion started: 7 January 2019

Atmospheric Measurement Techniques Discussions

Particles which are imaged by an OAP are fully in focus at the object plane, with image quality deteriorating as the particle location moves away from this object plane. The distance from the object plane that a particle can be observed is known as the depth of field (DoF) and is used to determine the instruments sample volume (together with the air speed and effective optical array width). Previous studies have found that the depth of field (at the 50% intensity level) follows a relationship of the form (Knollenberg, 1970)

$$DoF = \pm \frac{c{D_0}^2}{4\lambda}$$

Equation 1

where D_0 is the particle diameter and λ is the laser wavelength. c is a dimensionless constant, typically between 3 and 8 (Lawson et al., 2006; Gurganus & Lawson, 2018).

The size of the measured image depends on the particle's distance from the object plane. However, this dependence has been shown to be non-monotonic (Joe and List, 1987). Korolev et al. (1991) show that OAP images of transparent spheres (e.g. liquid drops) can be accurately approximated by the Fresnel diffraction from an opaque disc. The ratio of the detected image diameter to the actual physical diameter D_0 is purely a function of the normalised, dimensionless distance from the object plane Z_d,

$$Z_d = \frac{4\lambda Z}{{D_0}^2}$$

Equation 2

where Z is the distance from the object plane. The spatial intensity distributions from transparent spheres are independent of particle size. A distinct feature of these distributions is a bright spot at the centre of the image known as the Poisson spot. Korolev et al. (2007, hereafter K07) describes a method for determining a spherical particle's distance from the object plane and size using the size of the Poisson spot.

Joe and List (1986) suggested significantly reducing the depth of field so that the image size could be assumed to be equal to the particle size. Particles outside the new depth of field were identified using the ratio $A_{75\text{-}100}$ / ($A_{25\text{-}50}$ + $A_{50\text{-}75}$ + $A_{75\text{-}100}$). The disadvantage of reducing the depth of field in this way is that it can lead to poor sampling statistics. Similarly, by requiring at least one pixel to have a >67% decrease in detector signal Korolev et al. (1991) removes the most severely miss sized particles. Reuter & Bakan (1998, hereafter RB98) suggested an alternative approach by assuming a linear relationship between image size and the greyscale ratio $A_{25\text{-}50}$ / ($A_{25\text{-}50}$ + $A_{50\text{-}75}$ + $A_{75\text{-}100}$), which they then use to determine the particle size. This relationship was determined using laboratory experiments with a rotating disk with printed circular spots.

This paper describes tests on a Droplet Measurement Technologies Inc. (DMT) greyscale cloud imaging probe (CIP-15) using a droplet generation system. Liquid drops were injected into the probe at measured distances from the object plane to examine how this impacts the ability of the probe to accurately size particles. Results from these experiments are compared to synthetic images calculated assuming Fresnel diffraction (Korolev et al. 1991). Section 3.1 evaluates the efficacy of the K07 and RB98 size correction algorithms. Section 3.2 uses greyscale intensity ratios to determine a particle's distance from the object plane near the edge of the probe's depth of field. This allows significantly fragmented images to be removed and a revised depth of field to be used to determine particle concentrations. Section 3.4 examines how these results impact field measurements of particle size distributions using two research flights: one in a warm liquid cloud and one in cirrus.

2 Methods

2.1 Cloud imaging probe (CIP-15)

The CIP-15 is a commercially available greyscale OAP (DMT Inc., USA; Baumgardner et al., 2001). It has a 64 element photo-diode array with an effective pixel size of 15 µm, giving the probe a nominal size range of 15 to 960 µm. Images are recorded at three greyscale thresholds, which can be varied in the probe's data acquisition software. For the drop generator experiments these thresholds were set to 25, 50 and 75%; and 25, 50 and 67%. In Sect. 3.4.1 the thresholds were 40, 50 and 70%; and in Sect. 3.4.2 they were 25, 50 and 75%. The probe is fitted with anti-shatter tips to minimise ice shattering on the leading edge of the probe during field measurements. The measurements presented in this paper are from two CIP-15 systems. The major difference between the two probes is that one CIP-15 has an arm separation of 7 cm, and the other has an arm separation of 4 cm. The laboratory experiments and warm cloud results in Sect. 3.4.1 used the CIP with 7 cm arm separation, whereas the cirrus results in Sect. 3.4.2 use the CIP with 4 cm arm separation.

2.2 Supporting measurements

Section 3.4 compares measurements from the CIP-15 on board the FAAM Bae-146 research aircraft to those from a DMT Inc. Cloud Droplet Probe (CDP) and a holographic imaging probe. The CDP sizes particles in the range 3 to 50 µm using the scattered light intensity from a diode laser and assuming Mie scattering theory (Lance et al., 2010). The probe was calibrated during the campaign using glass calibration beads.

HALOHolo is a holographic imaging probe from the Institute for Atmospheric Physics at the University of Mainz and Max Planck Institute for Chemistry Mainz. It has a 6576 × 4384 pixel CCD detector with an effective pixel size of 2.95 µm. This equates to a sample volume of approximately 19×13×155 mm (~38 cm^3). At 6 frames per second and an average airspeed of about 100 ms^{-1}, this equates to a volume sample rate of ~230 cm^3 s^{-1}. Particles between 6 µm (2 pixels) and 1 cm (half the detector width) are resolvable in the hologram reconstructions. However, the detection of small particles is limited by noise in the background image. Therefore a minimum size threshold of 35 µm is applied, above which it is estimated that the probe's detection rate is greater than 90% (Schlenczek, 2017). Shattered particles were minimised by removing all particles with inter particle distances less than 10 mm (Fugal & Shaw, 2009; O'Shea et al., 2016)

2.3 Drop generator

A monodisperse stream of droplets was generated using a commercially available droplet generator. The generator is similar to that described by Lance et al. (2010) and uses piezoelectrically actuated printheads. Three MicroFab, Inc (USA) printheads with 60, 90 and 120 µm orifices were used during these experiments. Each printhead was in turn vertically mounted on two perpendicularly positioned translation stages (MTS50/M-Z8 - 50 mm, Thorlabs), each have 50 mm travel range and a 0.05 µm minimum increment. The printheads were connected to a fluid reservoir and the fluid pressure was adjusted using a pneumatic pressure controller so that the meniscus was at the end of the printhead. The printheads were actuated using a JetDrive III electronics module (MicroFab, Inc) to give a droplet production rate of 50 Hz.

The generation of a stable stream of monodisperse droplets depends on several factors, including the drive electronics and the physical properties of the fluid used. These factors

Atmos. Meas. Tech. Discuss., https://doi.org/10.5194/amt-2018-435
Manuscript under review for journal Atmos. Meas. Tech.
Discussion started: 7 January 2019

together with size of the printhead orifice control the size of the generated droplets. Previous work has shown that more stable outputs can be achieved using mixtures of water and ethylene glycol compared to using pure water (Jang et al., 2009; Liu, 2016). For these experiments, with the 60 µm printhead a 50% water and 50% ethylene glycol solution was used, while 100% ethylene glycol was used with the 90 µm and 120 µm printheads.

Figure 1 shows the setup for experiments that were performed on the CIP-15. The CIP-15 was vertically mounted below the drop generator. For each printhead the drop generator's position was stepped in 0.5 mm increments between the CIP-15's arms, dwelling for 3s after each movement.

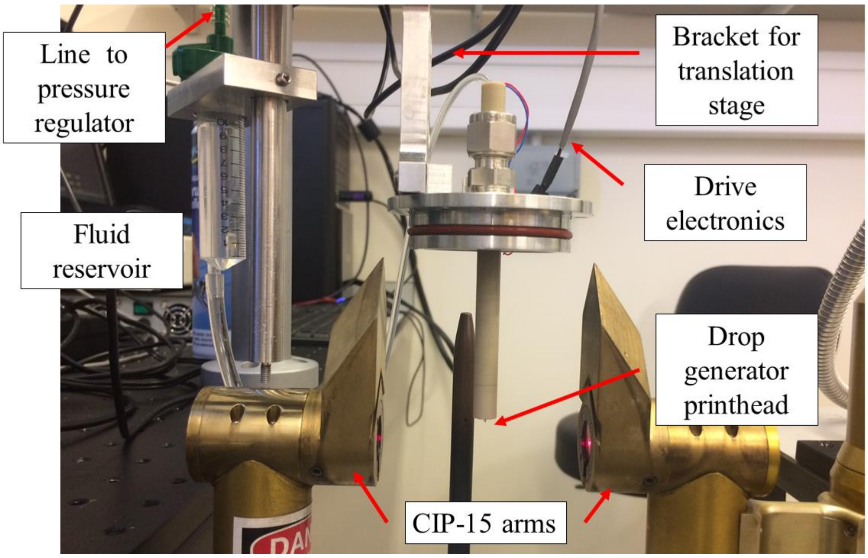

Figure 1. Photograph of the droplet generator and CIP-15.

To test the stability of the droplet generator separate experiments were performed where the droplets were monitored using a high speed camera (FASTCAM Mini AX, Photron, UK) with a zoom lens (Navitar, USA). The pixel size of the image for a given magnification was calibrated using a stage graticule (50 x 2 µm, Graticules Ltd, London, UK). The droplets were monitored for a 1 hour period at a droplet production rate of both 10 droplets s^{-1} and 250 droplets s^{-1}. The interquartile range of the drop diameters, as measured by the camera, were 2 µm and 3 µm, respectively.

Atmos. Meas. Tech. Discuss., https://doi.org/10.5194/amt-2018-435
Manuscript under review for journal Atmos. Meas. Tech.
Discussion started: 7 January 2019

2.4 Synthetic data

Modelled images were generated using optical, electronic, and diode thresholding simulations. The optical simulation considers only Fresnel diffraction by a round object, following the methods of Korolev et al. (1991) and K07. An electronic time delay simulation was also performed (Baumgardner and Korolev, 1997), but the effects are negligible due to the fast response of the electronics (tau = 51 ns) and the slow speed of the simulation (air speed of 10 m s^{-1}). The photodiodes are assumed to have a rectangular shape with a 5:4 aspect ratio and a 20% spacing between them, as in Korolev (2007). Similar to the drop generator experiments particles were injected at known distances from the object plane and the probe's response was simulated. This was done for particles with diameters 50 to 150 µm at intervals of 5 µm. These were positioned at 1 mm intervals over the range -5 to +5 cm from the object plane. Images were simulated using four different combinations of greyscale thresholds: 25, 50 and 75%; 30, 50 and 70%; 40, 50 and 70%; and 25, 50 and, 67%.

3 Results

3.1 Particle size correction

Figures 2-4 show the image diameter as a function of distance from the object plane. The diameters in these plots have been calculated along the axis of the optical array. Left panels show results from the laboratory experiments using the 60 µm, 90 µm and 120 µm drop generator printheads. Example images from the 90 µm printhead at three distances from the object plane are shown in Figure 5. Theoretically the size of the image at the centre of the object plane should be the closest approximation to the drop size. The median size of these are 60 µm, 90 µm and 90 µm for the 60 µm, 90 µm and 120 µm printheads, respectively. These measurements are subject to a 15 µm uncertainty due to the pixel resolution of the CIP-15. The right panels show similar plots for the synthetic data for 55 µm, 80 µm and 90 µm particles (dashed red lines). These sizes were chosen as they were the closest match to the droplet calibrations. The position of the depth of field as calculated using Eq.1 with a c value of 6 (blue) and 8 (green) are shown as vertical lines. If calculated correctly particles should not be visible outside the depth of field. If not removed, such particles would bias the measured

Atmos. Meas. Tech. Discuss., https://doi.org/10.5194/amt-2018-435
Manuscript under review for journal Atmos. Meas. Tech.
Discussion started: 7 January 2019

Atmospheric Measurement Techniques Discussions

concentrations. Figures 2-4 show that a c value of 8 effectively bounds the region where particles are visible using a 50% intensity threshold. The drop velocity will have an impact on this due to the probe's electronic time delay (Baumgardner and Korolev, 1997). These tests were performed with relatively slow droplet velocities (< 10 m s^{-1}), especially when compared to aircraft measurements (approximately 100 m s^{-1}). However, this effect is minimised by the fast time response of modern probes such as the CIP-15 (tau = 51 ns).

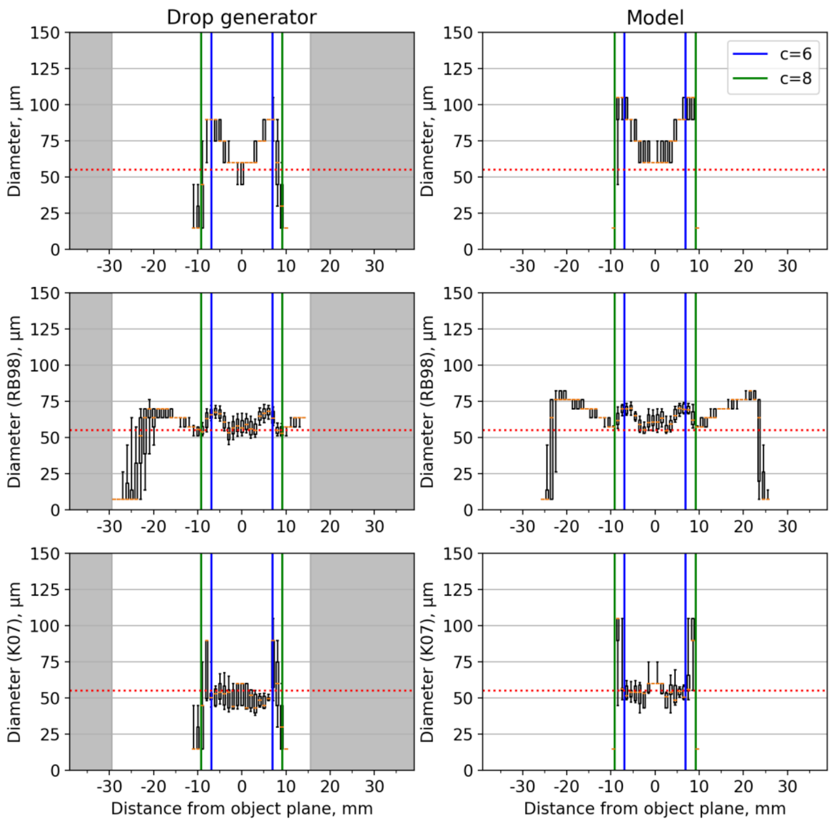

Figure 2. Box and whisker plots showing image diameter as a function of distance from the object plane. Left panels show results from the laboratory experiments using a 60 µm printhead. The grey shaded regions were not sampled using the drop generator. Right panels show the model image diameter from a 55 µm particle. Top panels show the image diameter using a 50%

decrease in intensity threshold (D_{50}). Middle panels show the diameter after the Reuter & Bakan (1998) size correction has been applied. Bottom panels show the diameter corrected using the Korolev et al. (2007) algorithm. Dashed red line shows the estimated droplet diameter. The position of the depth of field calculated using Eq. 1 with a c value of 6 (blue) and 8 (green) are shown as vertical lines.

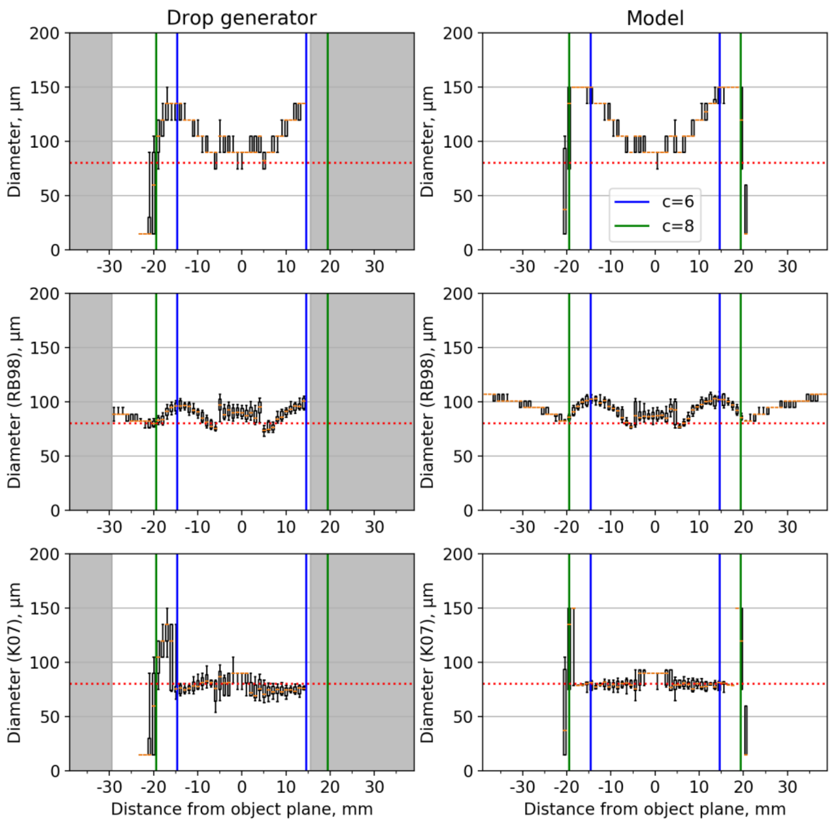

Figure 3. Same as Fig. 2 but left panels show results from the laboratory experiments using a 90 µm printhead and right panels show the modelled image diameter from an 80 µm particle.

Atmos. Meas. Tech. Discuss., https://doi.org/10.5194/amt-2018-435
Manuscript under review for journal Atmos. Meas. Tech.
Discussion started: 7 January 2019

Atmospheric Measurement Techniques
Open Access
Discussions

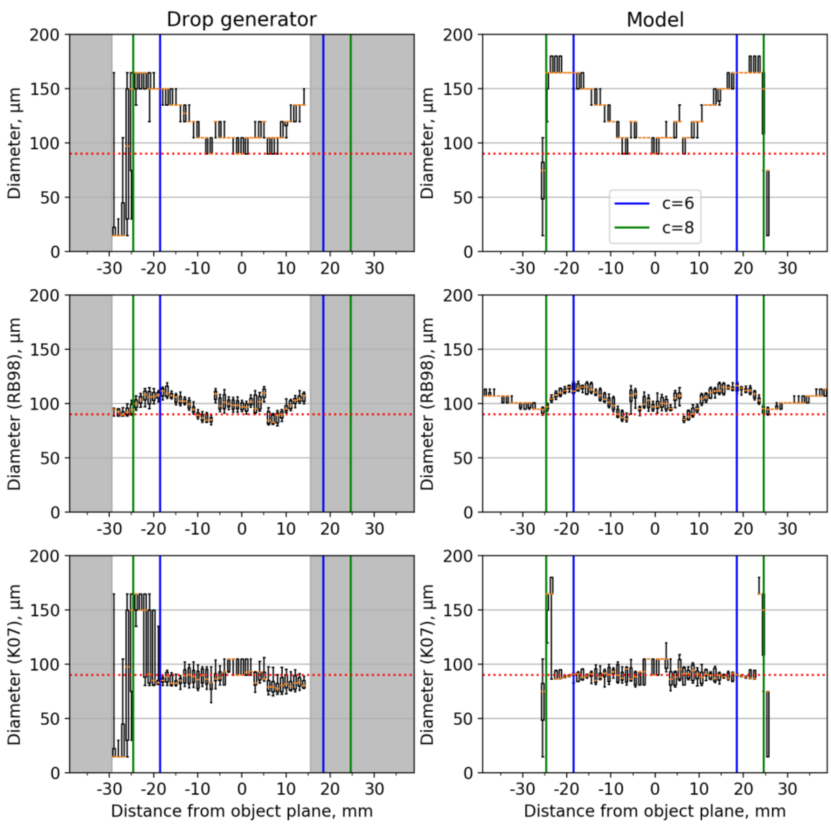

Figure 4. Same as Fig. 2 but left panels show results from the laboratory experiments using a 120 µm printhead and right panels show the modelled image diameter from a 90 µm particle.

Atmos. Meas. Tech. Discuss., https://doi.org/10.5194/amt-2018-435
Manuscript under review for journal Atmos. Meas. Tech.
Discussion started: 7 January 2019

Atmospheric Measurement Techniques
Discussions

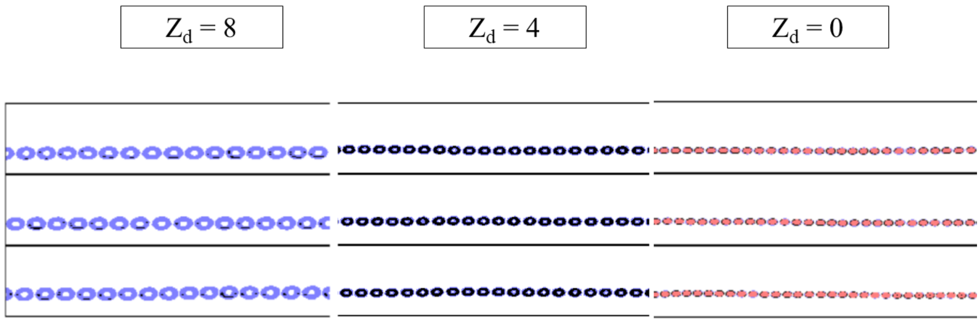

Figure 5. Example images of droplets from the droplet generator using a 90 μm printhead at Z_d = 8 (left), Z_d = 4 (middle) and Z_d = 0 (right). Decreases in detector intensity of 25 to 50%, 50 to 75% and >75% are shown as light blue, dark blue and orange pixels, respectively.

The middle panels show the image diameter as function of distance from the object plane once the RB98 size correction algorithm has been applied. This algorithm assumes a linear relationship between D_{25} and the greyscale ratio A_{25} / (A_{25} + A_{50} + A_{75}). In reality this relationship is not completely linear, as a result the corrected diameter is not independent of positon. Additionally there is a bias in the corrected size when compared to the particle model. To quantify this for the synthetic data we calculate the median of each position bin, Table 1 shows statistics for Z_d < 6. It is clear that the RB98 algorithm has a bias of the order 10 μm. A similar bias is seen in RB98 when compared to K07 if both algorithms are applied to results from the drop generator (Table 1).

Drop Generator					Model			
Printhead, μm	D_{50} (Z=0)	Image diameter, μm	Reuter & Bakan	Korolev et al. (2007),	Particle diameter, μm	Image diameter, μm	Reuter & Bakan	Korolev et al. (2007),

Atmos. Meas. Tech. Discuss., https://doi.org/10.5194/amt-2018-435
Manuscript under review for journal Atmos. Meas. Tech.
Discussion started: 7 January 2019

			(1997), µm				(1997), µm	
60	60	68 (15)	60 (10)	51 (10)	55	75 (26)	62 (9)	54 (7)
90	90	105 (30)	90 (11)	76 (8)	80	105 (32)	92 (13)	80 (4)
120	90	105 (23)	99 (7)	86 (7)	90	120 (43)	104 (15)	91 (5)

Table 1. Median (inter-quartile range) image diameter for $Z_d < 6$ from the drop generator experiments and the model images.

The lower panels in Figures 2-4 show the image diameter after the K07 algorithm has been applied. Across much of the depth of field this algorithm removes the image diameter's position dependence. For the synthetic data the median diameter across the depth of field is now within 1 µm of the true particle diameter and the inter-quartile range is reduced (Table 1). At the edge of the depth of field the Poisson spots become sufficiently large that the outer ring fragments at the 50% threshold (Fig. 5, left panel). Once this happens the K07 algorithm is not able to correct the size of these severely misshapen images. As shown in Figures 2-4 these fragmented images have large variability in their size and can be either much larger or smaller than the true particle size.

3.2 Identifying fragmented images

The K07 algorithm effectively corrects the diameter of imaged spherical particles across much of the depth of field for binary images at the 50% threshold. However for Z_d greater than approximately 7 the images are too fragmented and the correction no longer works effectively. These fragmented images need to be removed from further analysis, otherwise they will bias the measured size distributions.

The 1-D probes described Korolev et al. (1991) have an element of greyscale filtering. They do not record particle images, rather they just measure the diameter of particles using a 50% threshold. Only particles that have at least one detector with a >67% drop in detector intensity

Atmos. Meas. Tech. Discuss., https://doi.org/10.5194/amt-2018-435
Manuscript under review for journal Atmos. Meas. Tech.
Discussion started: 7 January 2019

are recorded. To test the efficacy of this approach to remove fragmented particles drop generator scans were performed with the CIP-15 thresholds set to 25, 50 and 67%. Figure 6 shows a size distribution of the K07 corrected diameter for a scan using the 60 µm printhead. The grey bars show data from all droplets, while the red markers show only images with at least one pixel above the 67% threshold. By performing this filtering the fragmented images are minimised and the depth of field is constrained to Z_d < 4.8.

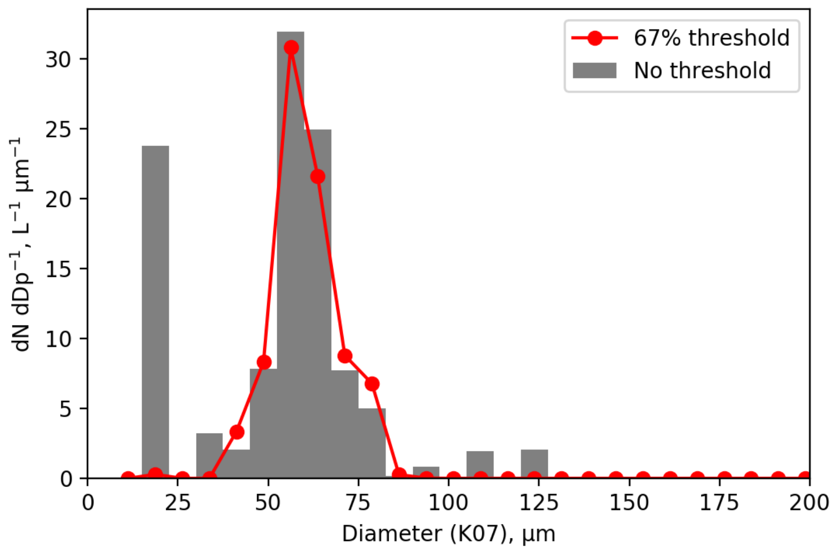

Figure 6. Size distribution of the K07 corrected diameter for a drop generator scan using the 60 µm printhead. The grey bars show data from all droplets, while the red markers show only images with at least one pixel with a >67% decrease in detector intensity. This reduces the depth of field to Z_d < 4.8.

Ideally greyscale information could be used to uniquely determine a particle's Z_d, which could either be used to correct the image size or exclude fragmented images from further analysis. Figure 7 shows various combinations of greyscale ratios as a function of Z_d. Results from the model for the particle sizes 50 to 150 µm are shown in grey, while results from the drop generator for the three printhead sizes (60, 90 and 120 µm) are shown in red. None of these

Atmos. Meas. Tech. Discuss., https://doi.org/10.5194/amt-2018-435
Manuscript under review for journal Atmos. Meas. Tech.
Discussion started: 7 January 2019

Atmospheric Measurement Techniques Discussions

ratios are monotonic and most exhibit very complex behaviour. As a consequence they can't easily be used to determine a particle's position across the whole depth of field. However, within certain regions some of the ratios are monotonic.

The ratio A_{50-75} / A_{25-50} (middle right panel) is near linear for the approximate range 3.5 < $|Z_d|$ < 8.5. This is an important region since it is where the images begin to fragment and the true particle size can no longer be accurately retrieved using the K07 algorithm. Before this ratio can be used to determine a particle's position we need to check that $|Z_d|$ is within the linear A_{50-75} / A_{25-50} region. If an image has A_{75-100} > 0 then $|Z_d|$ can be limited to less than approximately 3.5. Similarly, if A_{50-75} is equal to zero then $|Z_d|$ will be greater than approximately 8.5 and likely too fragmented for accurate sizing.

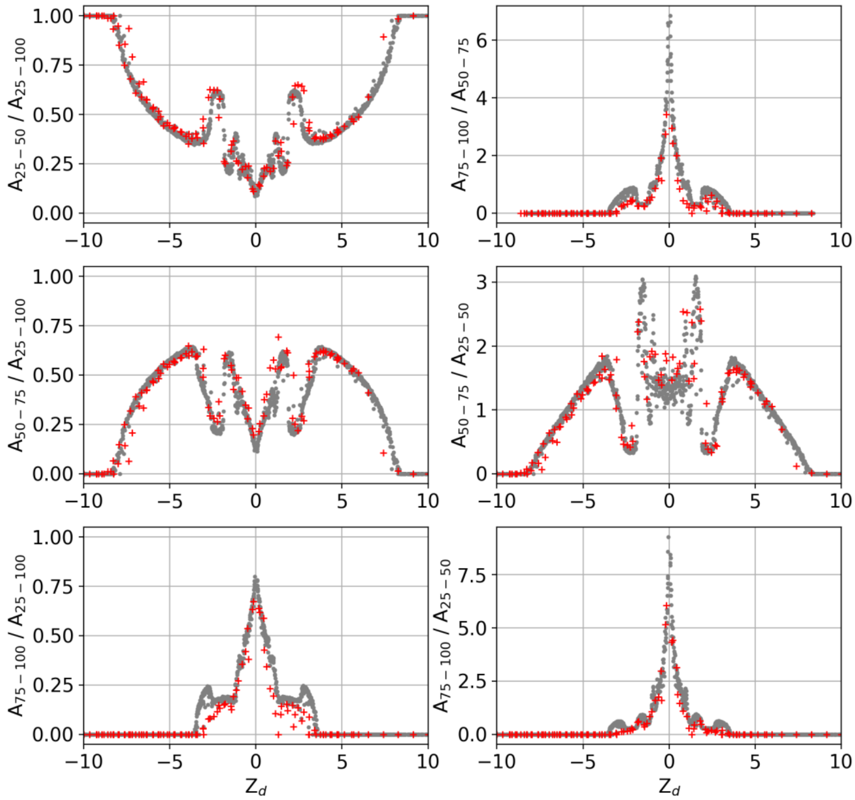

Figure 7. The ratios of the number of pixels between different thresholds from the drop generator experiments (red) and model simulations of particles in the size range 50 to 150 µm (grey) as a function of normalised distance from the object plane (Z_d).

Figure 8 shows results from the model (positive Z_d) that meet the criteria $A_{75\text{-}100} = 0$ and $A_{50\text{-}75} > 0$ (blue markers). The following equation can be fit to the data with an R^2 of 0.98,

$$|Z_d| = \frac{\frac{A_{50-75}}{A_{25-50}} - 3.2048}{-0.3772}$$

Atmos. Meas. Tech. Discuss., https://doi.org/10.5194/amt-2018-435
Manuscript under review for journal Atmos. Meas. Tech.
Discussion started: 7 January 2019

Atmospheric Measurement Techniques
Discussions

Equation 3

This equation allows the particle position to be retrieved over the approximate range $3.5 < |Z_d| < 8.5$. It should be noted that the uncertainty is greater for particles in the region $3.5 < |Z_d| < 5$ due to the larger number of outliers.

Figure 9 shows size distributions of the K07 corrected diameter for drop generator scans using the 60 µm (top panel), 90 µm (middle panel) and 120 µm (bottom panel) printheads. The grey bars show data from all droplets, while the coloured lines show size distributions that have been filtered using different Z_d thresholds. The Z_d of each droplet was determined using Eq. 3. By applying a Z_d threshold both the very large and very small outliers are removed from the size distribution.

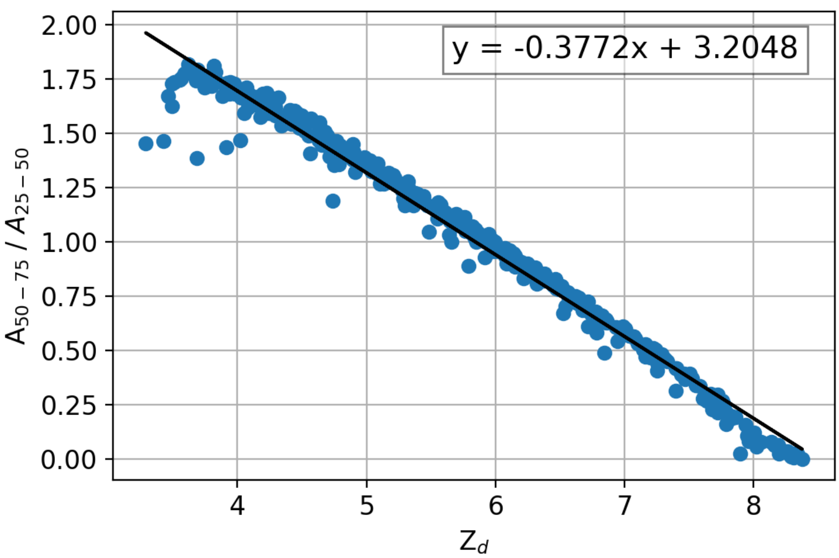

Figure 8. The ratio of the number of pixels between grayscale thresholds 50 – 75% and 25 – 50% (positive Z_d) that meet the criteria $A_{75\text{-}100} = 0$ and $A_{50\text{-}75} > 0$ (blue markers). This data is from model simulations of particles in the size range 50 to 150 µm.

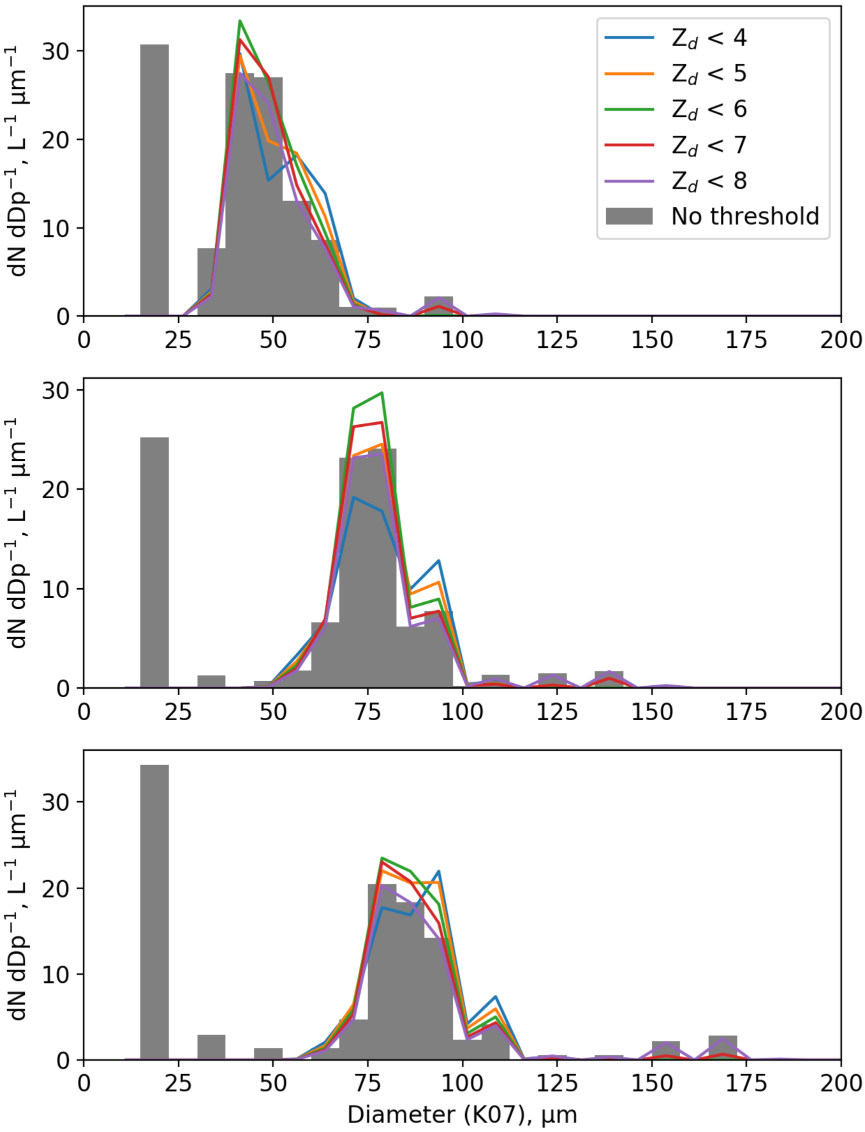
Z_d < 4
Z_d < 5
Z_d < 6
Z_d < 7
Z_d < 8
No threshold
dN dDp^{-1}, L^{-1} µm^{-1}
0
10
20
30
0
25
50
75
100
125
150
175
200
Diameter (K07), µm

1

Figure 9. Size distributions of the K07 corrected diameter for drop generator scans using the 60 µm (top panel), 90 µm (middle panel) and 120 µm (bottom panel) printheads. The grey bars show data from all droplets, while the coloured lines show size distributions that have been filtered using different Z_d thresholds. The Z_d of each droplet was determined using Eq. 3.

Similar relationships can be derived using different greyscale thresholds. We tested several different combinations of thresholds that could be used: first 40, 50 and 70%; second 30, 50 and 70%; and finally 25, 50 and 67%. A similar procedure was employed of first removing particles with no pixels above the highest threshold and ones without at least one pixel above the middle threshold. For each particle the number of pixels with greyscale intensity between the middle and upper threshold (A_{Mid}) was divided by the number of pixels between the lower and middle thresholds (A_{Low}). A linear equation of the following form was then fit to this ratio versus Z_d,

$$|Z_d| = \frac{\frac{A_{Mid}}{A_{Low}} + i}{j}$$

Equation 4

Table 2 shows the fit coefficients for the four different combinations of greyscale thresholds from the model data. Also shown is the approximate Z_d range where each relationship is applicable.

Greyscale thresholds			Coefficients		R^2	Z_d range
High	Mid	Low	i	j		
75	50	25	-3.2048	-0.3772	0.98	3.5 to 8.5
70	50	40	-7.8282	-0.9507	0.99	4.1 to 8.2
70	50	30	-4.0856	-0.4885	0.99	4.1 to 8.4
67	50	25	-3.3619	-0.4009	0.99	4.8 to 8.4

Table 2. Fit coefficients i and j for Eq. 4 for different combinations of greyscale thresholds.

Atmos. Meas. Tech. Discuss., https://doi.org/10.5194/amt-2018-435
Manuscript under review for journal Atmos. Meas. Tech.
Discussion started: 7 January 2019

Atmospheric Measurement Techniques Discussions

3.3 Sample volume

The previous section described how Z_d can be determined for images as they begin to fragment. This allows a threshold Z_d to be employed to remove these images from further analysis. To correctly determine the particle concentration the sample volume needs to be adjusted to take account of the Z_d threshold. The revised depth of field is calculated by setting c in Eq. 1 equal to the chosen Z_d threshold. For Z_d to be correctly calculated using Eq. 4 and the K07 size correction to be applicable the entire particle needs to be imaged. Images that have pixels greater than the low greyscale threshold in contact with the edge of the optical array should not be used to calculate the concentration. The probe sample volume (SVol) for a given D_0 can then be calculated using

$$SVol = TAS.\int_{-DoF}^{+DoF} (NR - D_{Low}(Z))\, dZ$$

Equation 5

where D_{Low} is the image diameter using all pixels greater the low greyscale threshold, TAS is the true air speed, N is the number of array elements and R is the resolution of the probe. This equation has been modified from Korolev et al. (1991) so that it uses D_{Low} rather than D_{50}. Across much of the probe's size range the D_{25} sample area is less than 10% smaller than the D_{50} sample area, however this increases for larger particles. The integration of the effective array width (NR- D_{Low}(Z)) is performed over whichever is smaller out of the depth of field or the probe arm width.

3.4 Airborne measurements

The following section applies the results from Sections 3.1 to 3.3 to field measurements from two research flights.

3.4.1 Liquid cloud

As part of the CLouds and Aerosol Radiative Impacts and Forcing (CLARIFY) project the FAAM Bae-146 Research Aircraft performed sorties out of Ascension Island. On 5 September 2017, Pockets of Open Cells were sampled. This flight was characterised by a clean marine boundary layer and large cloud droplets/drizzle. Figure 10a shows size distributions from the CIP-15 that have been averaged over a straight and level run at 14°C (16:42:10 to 16:43:15 GMT). Pink markers show the CDP size distribution averaged over the same period. The other coloured lines have been calculated using K07 using various Z_d thresholds. Figure 10b shows example CIP-15 images from this period. The particle diameters in this section have been calculated as the mean of the particle size along the axis of the optical array and the particle trajectory. Using a Z_d threshold less than 7 significantly reduces the concentration of drops smaller than 60 µm, which is in better agreement with the CDP. The decrease is over an order of magnitude for the smallest CIP-15 bin.

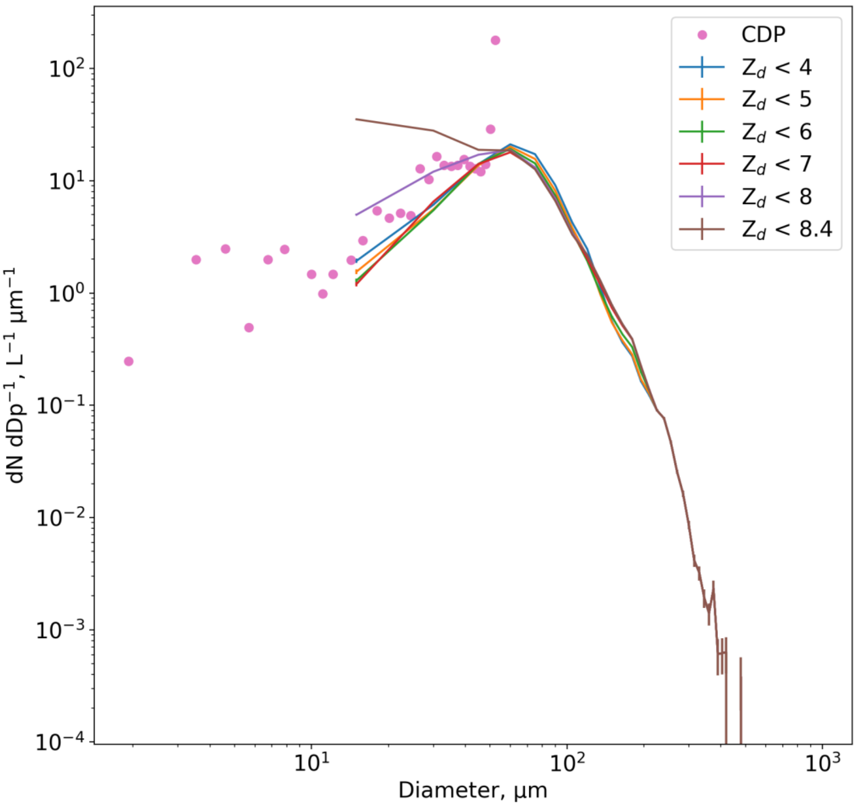

Figure 10a. Comparison in liquid cloud between the CDP and CIP-15 using different Z_d thresholds. Figure 10b) shows example CIP-15 images from this period. Decreases in detector intensity of 25 to 50%, 50 to 75% and >75% are shown as light blue, dark blue and orange pixels, respectively.

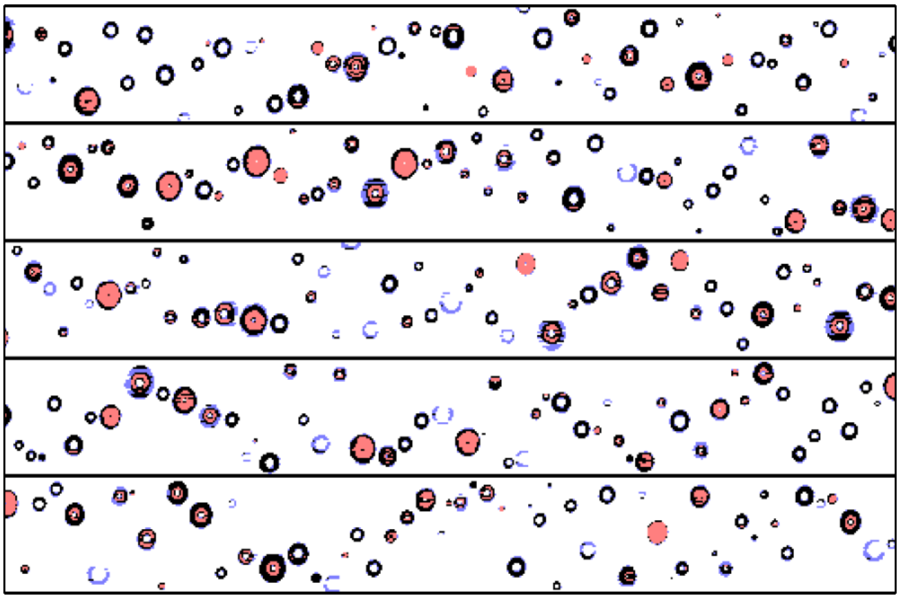

Figure 10b.

3.4.2 Cirrus

A number of studies have found a persistent small ice mode in their OAP measurements of cirrus clouds (Cotton et al., 2013; Jackson et al., 2015; O'Shea et al. 2016). O'Shea et al. (2016) hypothesised that in their measurements this was largely due to out of focus larger crystals. Due to the size dependence of the sample volume only a relatively small proportion of miss sized large particles are needed to cause a significant number concentration of small particles. The relationships between greyscale ratios and Z_d determined in this paper have been developed using spherical droplets. Similarly, K07 is strictly only applicable to spherical droplets. However, ice crystals can be a variety of complex shapes.

Atmos. Meas. Tech. Discuss., https://doi.org/10.5194/amt-2018-435
Manuscript under review for journal Atmos. Meas. Tech.
Discussion started: 7 January 2019

Atmospheric Measurement Techniques
Discussions

To examine whether the greyscale relationships in this paper can be applied to glaciated clouds we use measurements from the PICASSO project (Parameterizing Ice Clouds using Airborne obServationS and triple-frequency dOppler radar). On 7 February 2018, the FAAM BAe-146 sampled cirrus over southern UK. Figure 11a shows size distributions for a straight and level run at -42 °C (16:02:00 to 16:10:00 GMT). Crystals were predominantly rosettes and columns, with a smaller proportion of aggregates. Example CIP-15 images from this period are shown in Fig. 11b. Particles associated with inlet shattering were minimised by filtering particles with inter-arrival times less than $1x10^{-5}$ s (Field et al., 2006). The particles in Fig. 10a have not been corrected using K07.

Similar to O'Shea et al. (2016), if no Z_d filter is applied the CIP-15 cirrus size distribution is bimodal with one mode at approximately 200 µm and another at the smallest measured sizes. As a more restrictive Z_d threshold is applied the small particle mode (less than 100 µm) decreases. Similar to the liquid case (Section 3.4.1) the concentration of small particles decreases by an order of magnitude for $Z_d < 6$ compared to when no filtering is applied. However, this algorithm doesn't completely remove the small particle mode. There are a number of possible explanations for this: first, the mode may be real and due to ice nucleation. However, coincident holographic measurements do not show the small particle mode (pink markers, Fig. 11a), suggesting it is an artefact associated with the OAP measurement technique. Second, it may be due to shattering on the inlet of the probe. However as mentioned previously, shattering events should be associated with short inter-arrival times and a stringent inter-arrival threshold has been applied to this dataset. Third, noise in the CIP-15 images will degrade the accuracy of the Z_d retrieval. Finally, the non-spherical shape of ice crystals will mean that the greyscale relationships aren't directly applicable. Further work is needed to examine greyscale Z_d relationships for specific particle habits and whether a spherical approximation is applicable.

At large sizes the sample volume decreases with size till it is zero for particles larger than 960 µm. The Poisson counting uncertainty in the size distribution is shown as error bars in Fig. 10. As shown in Fig. 11 the number of counts becomes small and the counting uncertainty increases significantly for particles larger than approximately 700 µm.

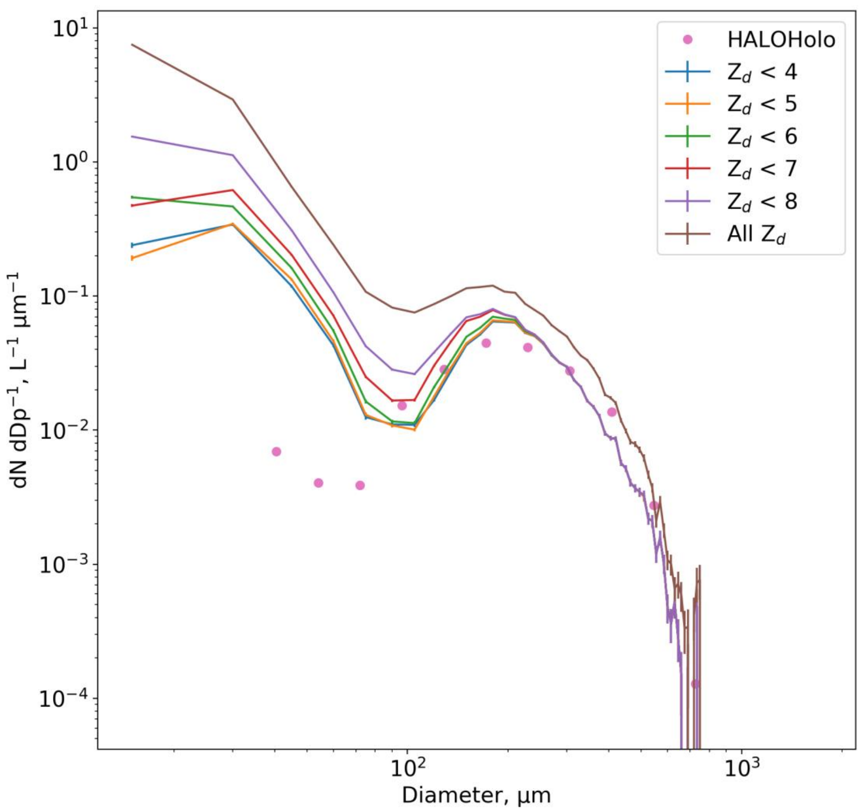

Figure 11a. CIP-15 size distribution in cirrus using different Z_d thresholds. Figure 10b shows example CIP-15 images from this period. Decreases in detector intensity of 25 to 50%, 50 to 75% and >75% are shown as light blue, dark blue and orange pixels, respectively.

Atmos. Meas. Tech. Discuss., https://doi.org/10.5194/amt-2018-435
Manuscript under review for journal Atmos. Meas. Tech.
Discussion started: 7 January 2019

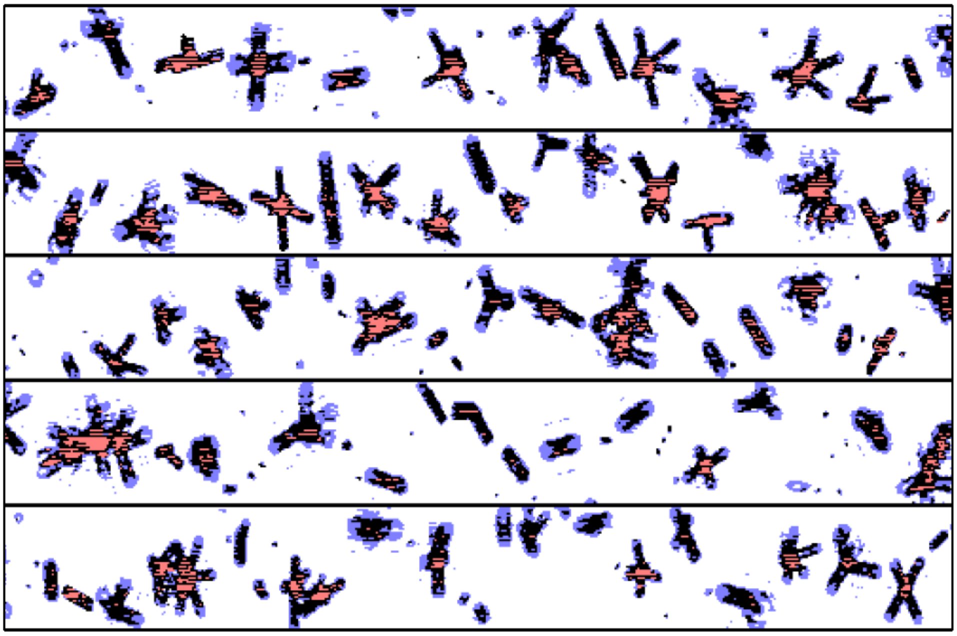

Figure 11b.

4 Conclusions

This paper has described tests on a grayscale OAP using a droplet generator, results from which have been compared to synthetic data. Despite recent advances in holographic instruments for cloud microphysical measurements (Fugal & Shaw, 2009) work is still needed to better characterise the uncertainties associated with this technique. Additionally holographic probes require high performance computers to post-process the significant amounts of data they generate (e.g. HALOHolo generated several terabytes per 2-5 hour flight during PICASSO). This makes it challenging to routinely deploy such instruments. Therefore it is likely that OAPs will be still widely used for at least another 10 years. We make the following recommendations for their use:

- K07 should be used to correct the image size of spherical particles. This algorithm is found to perform better than RB98 across much of the depth of field ($Z_d < 6$). However, K07 is not able to correct the size of the severely fragmented images of particles near the edge of the probe's depth of field ($Z_d > 6$).

- Fragmented images from particles near the edge of the depth of field need to be removed to avoid significant bias to the derived particle size distributions. This is particularly a problem for diameters less than approximately 100 µm due to the relatively small depth of field at these sizes.

- Greyscale information should be used to filter fragmented images and the probe's sample volume should be adjusted. The following four combinations of greyscale thresholds were tested: 25, 50 and 75%; 40, 50 and 70%; 30, 50 and 70%; and 25, 50 and 67%. Using these thresholds and the relationships presented in this paper it is possible to determine a particle's position near the edge of the depth of field. This methodology was tested on measurements from two research flights. In both cases this reduced the concentration of small particles (< 60 µm) by approximately an order of magnitude, significantly improving agreement with a Mie scattering spectrometer for the liquid case and with a holographic imaging probe for the cirrus case.

- The data from monoscale OAPs is unreliable below approximately 100 µm due to fragmented larger particles. A small number of monoscale probes exist that reject particles that do not have at least one detector with a >67% decrease in intensity. If this filtering is performed it would greatly minimise the impact of out-of-focus particles. However, this feature is not available on commonly used modern probes such as the 2DS (SPEC Inc., Lawson et al., 2006).

- Reintroducing a 67% intensity rejection criteria on monoscale probes should be a high priority if possible. If this requires hardware modifications, it may be more appropriate to upgrade to full grayscale capability.

- Past datasets from greyscale OAPs should be re-examined. The filtering and sample volume adjustments presented in this paper should be applied.

Data availability

The data presented here can be provided on request to the contact author.

Acknowledgements

The authors would like to thank Brian Derby, Andy Wallwork and Rachel Saunders for their assistance with the drop generator setup. We would like to thank Chris Westbrook and the PICASSO and CLARIFY teams for provision of the airborne data. Airborne data were obtained using the BAe-146-301 Atmospheric Research Aircraft (ARA) flown by Directflight Ltd and managed by the Facility for Airborne Atmospheric Measurements (FAAM), which is a joint entity of the Natural Environment Research Council (NERC) and the Met Office. The CIP-15s were provided by the National Centre for Atmospheric Science and FAAM. The National Centre for Atmospheric Science provided support for the droplet generator experiments. This work was supported by the NERC grants NE/P012426/1 and NE/L013584/1.

Atmos. Meas. Tech. Discuss., https://doi.org/10.5194/amt-2018-435
Manuscript under review for journal Atmos. Meas. Tech.
Discussion started: 7 January 2019

References

Baumgardner, D., Jonsson, H., Dawson, W., O'Connor, D., and Newton, R.: The cloud, aerosol and precipitation spectrometer: a new instrument for cloud investigations, Atmos. Res., 59–60, 251–264, https://doi.org/10.1016/S0169-8095(01)00119- 3, 2001.

Baumgardner, D. and Korolev, A.: Airspeed Corrections for Optical Array Probe Sample Volumes, J. Atmos. Ocean. Tech., 14, 1224–1229, https://doi.org/10.1175/1520-0426(1997)014<1224:ACFOAP>2.0.CO;2, 1997.

Cotton, R. J., Field, P. R., Ulanowski, Z., Kaye, P. H., Hirst, E., Greenaway, R. S., Crawford, I., Crosier, J., and Dorsey, J.: The effective density of small ice particles obtained from in situ aircraft observations of mid-latitude cirrus, Q. J. Royal Meteor. Soc., 139, 1923–1934, 2013.

Field, P. R.: Aircraft Observations of Ice Crystal Evolution in an Altostratus Cloud, Journal of the Atmospheric Sciences, 56, 1925–1941, https://doi.org/10.1175/1520-0469(1999)056<1925:AOOICE>2.0.CO;2, 1999.

Field, P. R., Heymsfield, A. J., and Bansemer, A.: Shattering and Particle Interarrival Times Measured by Optical Array Probes in Ice Clouds, J. Atmos. Oceanic Technol., 23, 1357–1371, 2006.

Fox, S., Mendrok, J., Eriksson, P., Ekelund, R., O'Shea, S. J., Bower, K. N., Harlow, R. C., and Pickering, J. C.: Airborne validation of radiative transfer modelling of ice clouds at millimetre and sub-millimetre wavelengths, Atmos. Meas. Tech. Discuss., https://doi.org/10.5194/amt-2018-308, in review, 2018.

Fugal, J. P. and Shaw, R. A.: Cloud particle size distributions measured with an airborne digital in-line holographic instrument, Atmos. Meas. Tech., 2, 259-271, https://doi.org/10.5194/amt-2-259-2009, 2009.

Gurganus, C., and Lawson, P.: Laboratory and flight tests of 2D imaging probes: Toward a better understanding of instrument performance and the impact on archived data, J. Atmos. Oceanic Technol. 35, 7, 1533-1553, doi: 10.1175/JTECH-D-17-0202.1, 2018.

Jackson, R. C., McFarquhar, G. M., Fridlind, A. M., and Atlas, R.: The dependence of cirrus gamma size distributions expressed as volumes in N0-λ-μ phase space and bulk cloud properties on environmental conditions: Results from the Small Ice Particles in Cirrus Experiment (SPARTICUS), J. Geophys. Res.-Atmos., 120, 10351–10377, doi:10.1002/2015JD023492, 2015.

Jang, D., Kim, D., Moon, J.: Influence of fluid physical properties on ink-jet printability. Langmuir, 25, 2629–2635, 2009.

Joe, P., and List, R.: Testing and performance of two dimensional optical array spectrometers with greyscale, J. Atmos. Oceanic Technol., 4, 139–150, 1987.

Knollenberg, R. G.: The optical array: An alternative to scattering or extinction for airborne particle size determination, J. Appl. Meteorol., 9, 86–103, doi:10.1175/1520-0450(1970)009<0086:TOAAAT>2.0.CO;2, 1970.

Korolev, A.: Reconstruction of the sizes of spherical particles from their shadow images. Part I: Theoretical considerations, J. Atmos. Ocean. Tech., 24, 376–389, 2007.

Korolev, A. V., Emery, E. F., Strapp, J. W., Cober, S. G., Isaac, G. A., Wasey, M. and Marcotte, D.: Small ice particles in tropospheric clouds: Fact or artifact? Airborne icing instrumentation evaluation experiment, Bull. Am. Meteorol. Soc., 92(8), 967–973, doi:10.1175/2010BAMS3141.1, 2011.

Korolev, A. V, Kuznetsov, S. V., Makarov, Yu. E., and Novikov, V. S.: Evaluation of measurements of particle size and sample area from optical array probes. J. Atmos. Oceanic Technol., 8, 514–522, 1991.

Lance, S., Brock, C. A., Rogers, D. and Gordon, J. A.: Water droplet calibration of the Cloud Droplet Probe (CDP) and in-flight performance in liquid, ice and mixed-phase clouds during ARCPAC, Atmos. Meas. Tech., 3(6), 1683–1706, doi:10.5194/amt-3-1683-2010, 2010.

Lawson, R. P., O'Connor, D., Zmarzly, P., Weaver, K., Baker, B., Mo, Q. and Jonsson, H.: The 2D-S (stereo) probe: Design and preliminary tests of a new airborne, high-speed, high-resolution particle imaging probe, J. Atmos. Ocean. Technol., 23(11), 1462–1477, doi:10.1175/JTECH1927.1, 2006.

Lawson, R. P., Woods, S., and Morrison, H.: The Microphysics of Ice and Precipitation Development in Tropical Cumulus Clouds, J. Atmos. Sci., 72, 2429–2445, doi:10.1175/JAS-D-14-0274.1, 2015.

Liu, Y.: Inkjet printed drops and three-dimensional ceramix structures, PhD Thesis, University of Manchester, 2016.

Mace, G., G., and Benson, S.: Diagnosing cloud microphysical process information from remote sensing measurements: A feasibility study using aircraft data. Part I: Tropical anvils measured during TC4. J. Appl. Meteor. Climatol., 56, 633–649, https://doi.org/10.1175/JAMC-D-16-0083.1, 2017.

O'Shea, S. J., Choularton, T. W., Lloyd, G., Crosier, J., Bower, K. N., Gallagher, M., Abel, S. J., Cotton, R. J., Brown, P. R. A., Fugal, J. P., Schlenczek, O., Borrmann, S., and Pickering, J. C.: Airborne observations of the microphysical structure of two contrasting cirrus clouds, J. Geophys. Res., 121, 13, https://doi.org/10.1002/2016JD025278, 2016.

Reuter, A. and Bakan, S.: Improvements of cloud particle sizing with a 2-D-grey probe, J. Atmos. Ocean. Tech., 15, 1196–1203, 1998.

Schlenczek, O.: Airborne and ground-based holographic measurement of hydrometeors in liquid-phase, mixed-phase and ice clouds, PhD Thesis, University of Mainz, 2017.

Wendisch, M. and Brenguier, J.-L. (Eds.): Airborne Measurements for Environmental Research: Methods and Instruments., vol. ISBN: 978-3-527-40996-9, Wiley-VCH Verlag GmbH & Co. KGaA, Weinheim, Germany, 2013.